

# 山东蓬莱石家金矿床载金黄铁矿热电性、晶胞参数 及其找矿意义<sup>\*</sup>

冯李强<sup>1</sup>, 顾雪祥<sup>2,3\*\*</sup>, 章永梅<sup>2,3</sup>, 沈睿文<sup>1</sup>, 张英帅<sup>2</sup>, 王鹏飞<sup>1</sup>, 王大伟<sup>1</sup>

(1 中国地质调查局自然资源综合调查指挥中心, 北京 100055; 2 中国地质大学(北京)地球科学与资源学院, 北京 100083;

3 中国地质大学(北京)地质过程与矿产资源国家重点实验室, 北京 100083)

**摘要** 石家金矿床位于胶东中部蓬莱-栖霞成矿带北段, 是一个赋存于中生代花岗岩中受构造带控制的石英脉型金矿床。由于多年开采, 矿区浅部资源已近于枯竭, 亟需向深部拓展找矿空间。黄铁矿是石家金矿床最常见的金属矿物, 也是最重要的载金矿物, 其标型特征对深部找矿预测具有十分重要的意义。文章对采自石家金矿床326号矿脉不同海拔高主成矿阶段黄铁矿的热电性与晶胞参数进行了分析, 结果表明: 在-595~165 m 标高内, 石家金矿床黄铁矿的热电导型以P型为主, 占比约97.5%, 表明目前揭露的矿体处于矿化系统的上部或顶部; 热电系数( $\alpha$ )变化于-288.3~304.9  $\mu\text{V}/\text{C}$ , 较大的离散范围表明矿体垂向延伸较大; 黄铁矿热电系数离散度为8%~68%, 较低的离散度指示黄铁矿形成于较为稳定的条件之下, 并且矿化程度较好; 利用热电系数计算黄铁矿的形成温度集中于210~250°C, 指示石家金矿床属于中温矿床; 根据热电系数计算的矿体剥蚀率( $\gamma$ )为25.5%~34.0%, 表明矿体未遭受大规模的剥蚀, 向下仍有较大延伸。黄铁矿晶胞参数 $a_0$ 介于0.5418~0.5422 nm, 略大于理论值(0.54176 nm)。结合黄铁矿热电导型与前人研究, 认为晶胞参数的变大可能与As类质同象替代S有关。综合分析认为, 石家金矿床在-600 m 以下的深部仍具有良好的找矿前景。

**关键词** 黄铁矿; 热电性; 晶胞参数; 深部找矿预测; 石家金矿; 胶东

中图分类号:P618.51

文献标志码:A

## Thermoelectricity and cell parameters of gold-bearing pyrite and their significance for prospecting of Shijia gold deposit in Penglai, Shandong Province

FENG LiQiang<sup>1</sup>, GU XueXiang<sup>2,3</sup>, ZHANG YongMei<sup>2,3</sup>, SHEN RuiWen<sup>1</sup>, ZHANG YingShuai<sup>2</sup>,  
WANG PengFei<sup>1</sup> and WANG DaWei<sup>1</sup>

(1 Command Center of Natural Resources Comprehensive Survey, China Geological Survey, Beijing 100055, China; 2 School of Earth Sciences and Resources, China University of Geosciences, Beijing 100083, China; 3 State Key Laboratory of Geological Processes and Mineral Resources, China University of Geosciences, Beijing 100083, China)

### Abstract

The Shijia gold deposit is located in the north of the Penglai-Qixia gold belt in the central part of Jiaodong Peninsula. It is a quartz-vein type gold deposit that occurs in the Mesozoic granite and is controlled by structural zones. Due to years of mining, the shallow resources in the mining area have been almost mined out, and there is an urgent need to expand the exploration space to the deeper part. Pyrite is the most common metal mineral and the most important gold-bearing mineral in the Shijia gold deposit. Its typomorphic characteristics are of great sig-

\* 本文得到国家自然科学基金重点项目“新疆西天山北缘晚古生代斑岩-矽卡岩型铜钼铁多金属成矿与岩浆-热液作用过程”(编号: 42130804)和中国地质调查局地质调查专项“全国金矿勘查成果集成与战略选区”(编号: DD20230374)联合资助

第一作者简介 冯李强, 1991年生, 男, 博士, 工程师, 从事矿床学及矿床地球化学研究。Email: fengliqiang@mail.cgs.gov.cn

\*\* 通讯作者 顾雪祥, 1963年生, 男, 教授, 博士生导师, 主要从事矿床学与矿床地球化学研究。Email: xuexiang\_gu@cugb.edu.cn

收稿日期 2023-05-01; 改回日期 2023-08-24。张绮玲编辑。

nificance to the deep prospecting and prediction of the Shijia gold deposit. This paper systematically analyzes the thermoelectricity of the main-ore stage pyrite from No. 326 orebody of the Shijia gold deposit at different altitudes. The results show that the thermoelectric conduction type of pyrite in the Shijia gold deposit is dominated by P-type, which accounts for about 97.5% in the elevation range of -595~165 m, indicating that the currently mined orebody is at the upper or top of the mineralization system. The thermoelectric coefficient ( $\alpha$ ) has a large discrete range, ranging from -288.3 to 304.9  $\mu\text{V}/^\circ\text{C}$ , indicating a significant vertical extension of the orebody. The dispersion of thermoelectric coefficient is 8%~68%, and the lower dispersion indicates that pyrite is formed under relatively stable conditions and has a good mineralization. The formation temperature of pyrite calculated by thermoelectric coefficient is concentrated between 210°C to 250°C, indicating that the Shijia gold deposit is a medium temperature deposit. Orebody denudation rate ( $\gamma$ ) calculated according to thermoelectric coefficient ranges from 25.5% to 34.0%, indicating that the orebody has not been significantly eroded and still extends to the deep. The cell parameter ( $a_0$ ) of pyrite is between 0.5418 nm and 0.5422 nm, slightly greater than the theoretical value of 0.54176 nm. Combined with the thermoelectric conduction type of pyrite and previous research, it is considered that the enlargement of cell parameter may be related to the isomorphic substitution of As and Sb for S. The above results clearly indicate that there is still a good prospecting potential in the deeper part below -600 m in the Shijia gold deposit.

**Keywords:** pyrite, thermoelectricity, cell parameters, deep prospecting prediction, Shijia gold deposit, Jiaodong

黄铁矿是众多热液矿床中最为常见、占比最高的硫化物,也是金矿床中最重要的载金矿物(顾雪祥等,2019;申俊峰等,2021)。作为一种半导体矿物,黄铁矿的热电性与其形成的物理化学条件密切相关,对于判断成矿温度、矿床规模及寻找隐伏矿体等方面具有重要意义(申俊峰等,2013),目前已作为一种非常实用且有效的找矿方法用于指导金矿深部及外围找矿预测。黄铁矿的晶胞参数也是其重要的物理标型特征之一,并且会随着晶体化学组成和外界环境的某些变化而发生有规律的微小变化(高永伟等,2019),也有助于指导找矿和分析矿床成因(曹烨等,2010)。

胶东地区是中国著名的金矿集区和黄金产地,累计探明黄金储量超过 5000 t(宋明春等,2020)。区内由西至东依次分布着招远-莱州、蓬莱-栖霞以及牟平-乳山 3 大金矿带(范洪瑞等,2016)。位于蓬莱-栖霞成矿带北段的大柳行地区在大地构造位置属于华北克拉通东南缘的胶北隆起区,区内金矿资源丰富,分布着黑岚沟、河西、石家等石英脉型金矿床(图 1)。本文所研究的石家金矿床是一个储量超过 10 t 的中型金矿床。随着多年的开采,矿区浅部资源已近于枯竭,找矿空间亟需向深部拓展。由于该矿区地表覆盖严重,地表地质信息不丰富,在一定程度上限制了矿区的找矿进程。原生晕研究表明,矿体具有向

南侧伏的特点,矿区南段为成矿的有利部位(张英帅等,2021)。因此,为了进一步查明矿区深部资源状况,明确找矿方向,延长矿山服务年限,本文系统分析了石家金矿床 326 号主矿脉南段主成矿阶段的黄铁矿的热电性与晶胞参数特征,探讨了其对矿床形成温度和矿体剥蚀程度的指示意义,为该矿床的深部成矿预测和资源潜力评价提供一定的依据。

## 1 区域与矿床地质

大柳行地区出露地层简单,以新太古界胶东群、古元古界荆山群和粉子山群以及新元古界蓬莱群等前寒武纪变质基底为主。中生界仅小范围出露,由下白垩统莱阳群和青山群组成,两者不整合于前寒武纪基底之上。区内断裂构造发育,以一系列近平行展布的 NNE 向断层为主,并控制了区内矿脉、蚀变带以及矿体的产出。中生代花岗岩广泛分布,以虎路线断裂为界,西侧为早白垩世郭家岭含角闪二长花岗岩(130~126 Ma; Yang et al., 2012; Li et al., 2019),东侧为晚侏罗世玲珑二长花岗岩(165~150 Ma; Ma et al., 2013; Yang et al., 2014)。新太古代和古元古代的侵入岩呈小规模岩株出露于区域南部,岩性包括变辉长岩、片麻状花岗岩等。

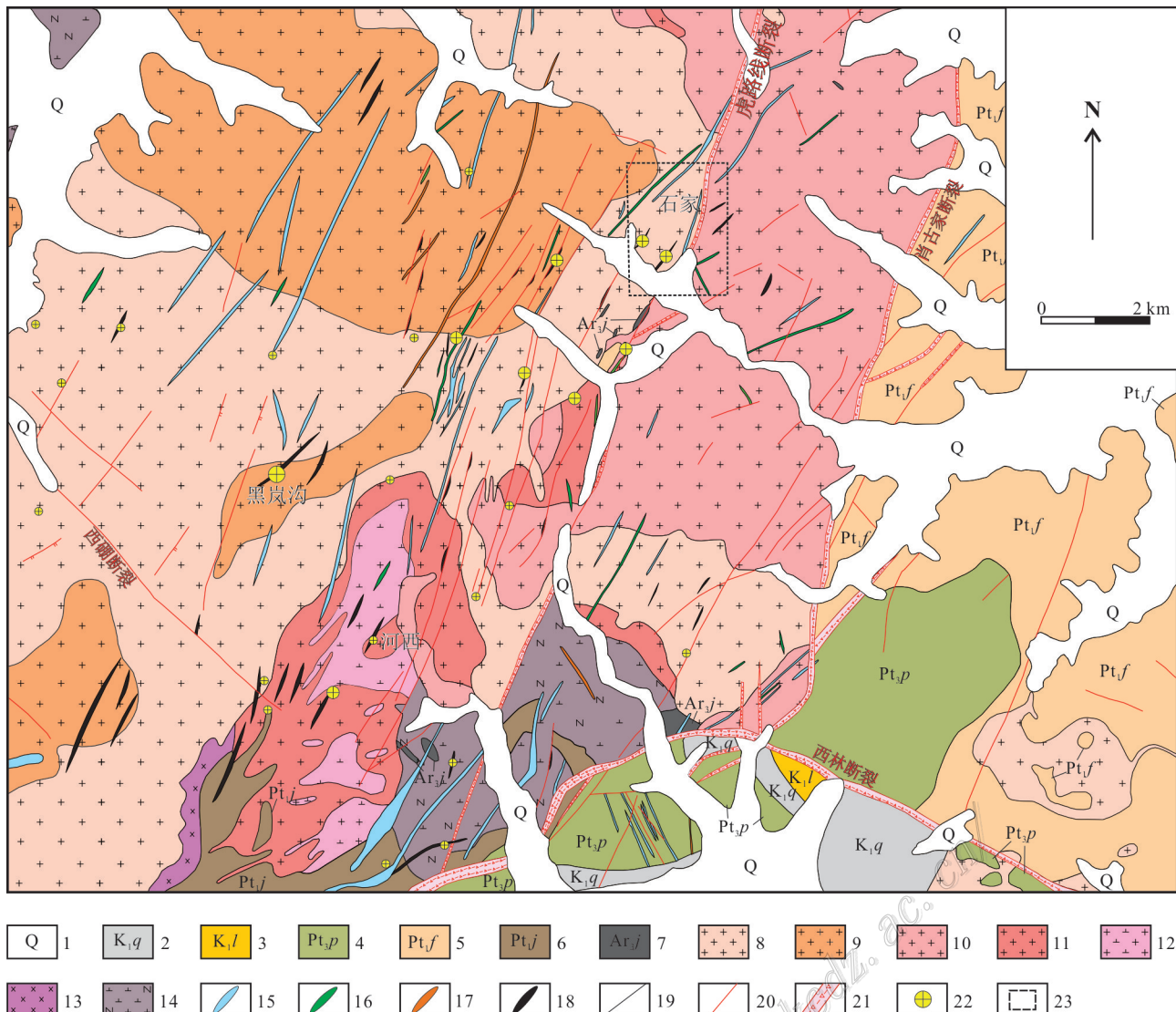


图1 大柳行地区地质简图(据Feng et al., 2020修改)

1—第四系; 2—下白垩统青山群; 3—下白垩统莱阳群; 4—新元古界蓬莱群; 5—古元古界粉子山群; 6—古元古界荆山群; 7—新太古界胶东群; 8—早白垩世郭家岭含角闪石二长花岗岩; 9—早白垩世郭家岭含黑云母二长花岗岩; 10—晚侏罗世玲珑二长花岗岩; 11—古元古代花岗岩; 12—新太古代花岗岩; 13—新太古代变质辉长岩; 14—新太古代英云闪片麻岩; 15—早白垩世辉绿岩脉; 16—早白垩世煌斑岩脉; 17—早白垩世正长斑岩脉; 18—金矿脉; 19—地质界线; 20—断层; 21—构造断裂带; 22—金矿床; 23—研究区

Fig. 1 Regional geological sketch map of the Daluhang area (modified from Feng et al., 2020)

1—Quaternary sediments; 2—Lower Cretaceous Qingshan Group; 3—Lower Cretaceous Laiyang Group; 4—Neoproterozoic Penglai Group; 5—Paleoproterozoic Fenzishan Group; 6—Paleoproterozoic Jingshan Group; 7—Neoarchean Jiaodong Group; 8—Early Cretaceous Guojialing hornblende-bearing monzogranite; 9—Early Cretaceous Guojialing biotite-bearing monzogranite; 10—Late Jurassic Linglong monzogranite; 11—Paleoproterozoic granitoids; 12—Neoarchean granitoids; 13—Neoarchean metagabbro; 14—Neoarchean tonalitic gneiss; 15—Early Cretaceous diorite porphyry dykes; 16—Early Cretaceous lamprophyre dykes; 17—Early Cretaceous syenite porphyry dykes; 18—Gold vein; 19—Geological boundary; 20—Fault; 21—Structural fault zone; 22—Gold deposit; 23—Study area

区内早白垩世酸性-基性脉岩发育,主要包括花岗伟晶岩、煌斑岩、辉绿岩、花岗斑岩等,呈脉状平行或垂直于矿体产出,并且与金矿体具有紧密的时空联系。岩石地球化学研究表明,矿区煌斑岩与辉绿

岩起源于富集岩石圈地幔部分熔融,花岗斑岩则与幔源岩浆底侵背景下杂砂岩部分熔融有关(石启慧等,2023)。

目前在石家金矿床共圈定13条矿体,1号脉、

326号脉及334号脉是规模最大的3条矿脉,占矿石储量的98%以上。三条矿脉均赋存于郭家岭含角闪二长花岗岩之中,整体上呈近平行、等间距分布(图2)。

1号脉位于矿区西部,分布于4~100线之间。矿区控制最长1010 m,最大斜深1030 m,矿体厚度0.15~2.30 m,平均厚度0.90 m。矿体走向350°~

25°,倾向南东,倾角陡立,为61°~89°,平均76°。矿化比较连续,是矿区规模最大的矿体,占矿石储量的48%,矿石Au品位为1.00~41.54 g/t,平均5.60 g/t。

326号脉位于1号脉以东100~200 m处,由于矿化不连续,分为326-2和326-3两条矿体。326-2号矿体位于矿区北侧,分布于72~112线之间,矿区沿

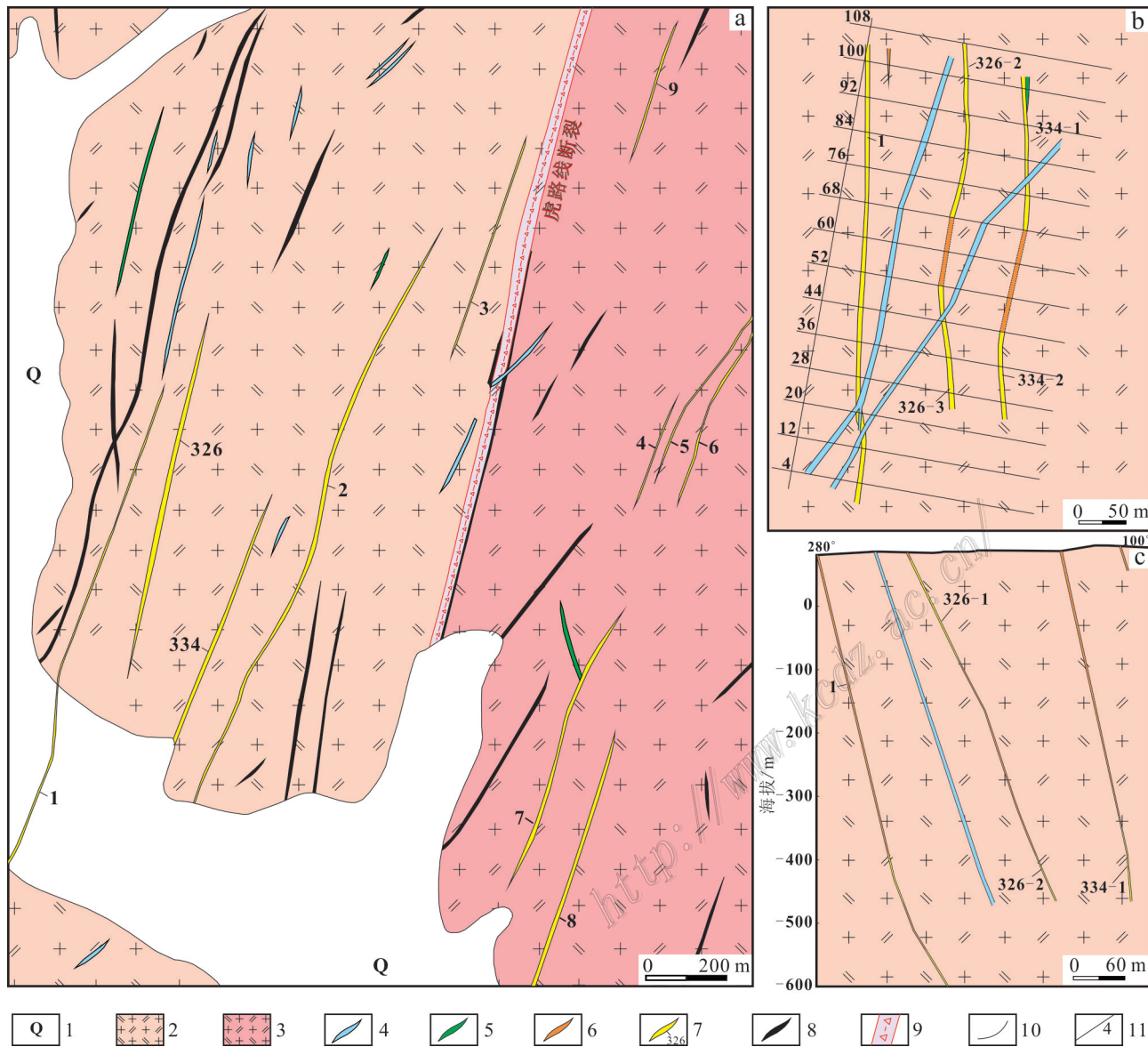


图2 石家金矿区地质图(a)、-400 m中段平面图(b)及84号勘探线剖面图(c)(据Feng et al., 2020修改)

1—第四系;2—郭家岭二长花岗岩;3—玲珑二长花岗岩;4—辉绿岩脉;5—煌斑岩脉;6—黄铁绢英化碎裂岩;7—矿体;8—石英脉;9—构造断裂带;10—地质界线;11—勘探线及其编号

Fig. 2 Schematic geology of the Shijia gold deposit(a), plan view of -400 m level(b) and cross-section of prospecting line 84(c)  
(modified from Feng et al., 2020)

1—Quaternary; 2—Guojialing monzogranite; 3—Linglong monzogranite; 4—Diabase dykes; 5—Lamprophyre dykes; 6—Beresitization cataclasite; 7—Orebody; 8—Quartz vein; 9—Tectonic fault zone; 10—Geological boundary; 11—Exploration line and its number

走向控制最长350 m,最大斜深910 m。矿化比较连续,占矿石储量的15%。该矿体厚度0.17~1.92 m,平均厚度0.82 m,Au品位为1.10~273.88 g/t,平均品位6.60 g/t。326-3号矿体位于矿区南侧,分布于20~52线之间,控制长度310 m,最大斜深520 m,厚0.18~1.59 m,平均厚度0.75 m。矿化连续,占矿石储量的14%,Au品位为1.00~176.50 g/t,平均品位8.62 g/t。两条矿体均呈近南北展布,走向主要集中于355°~5°,倾向南东,倾角介于57°~90°。

334号脉位于326号脉东侧200~300 m处,分为334-1和334-2两条矿体。北侧的334-1号矿体分布

于72~104号勘探线之间,矿区内控制最长280 m,最大斜深360 m,矿体厚度0.19~2.02 m,平均厚度0.77 m,Au品位介于1.20~60.00 g/t,平均品位10.78 g/t。南侧的334-2号矿体分布于4~52号勘探线之间,控制最长250 m,最大斜深640 m。该矿体厚度0.28~1.32 m,平均厚度0.78 m,Au品位1.00~72.20 g/t,平均品位7.72 g/t。矿体呈近南北向的脉体产出,倾向75°~109°,倾角介于56°~90°。

矿石类型以石英-硫化物脉型为主,其次为蚀变岩型(图3a~c)。金属矿物主要包括黄铁矿、闪锌矿、方铅矿,少量的黄铜矿和自然金;非金属矿物主要为

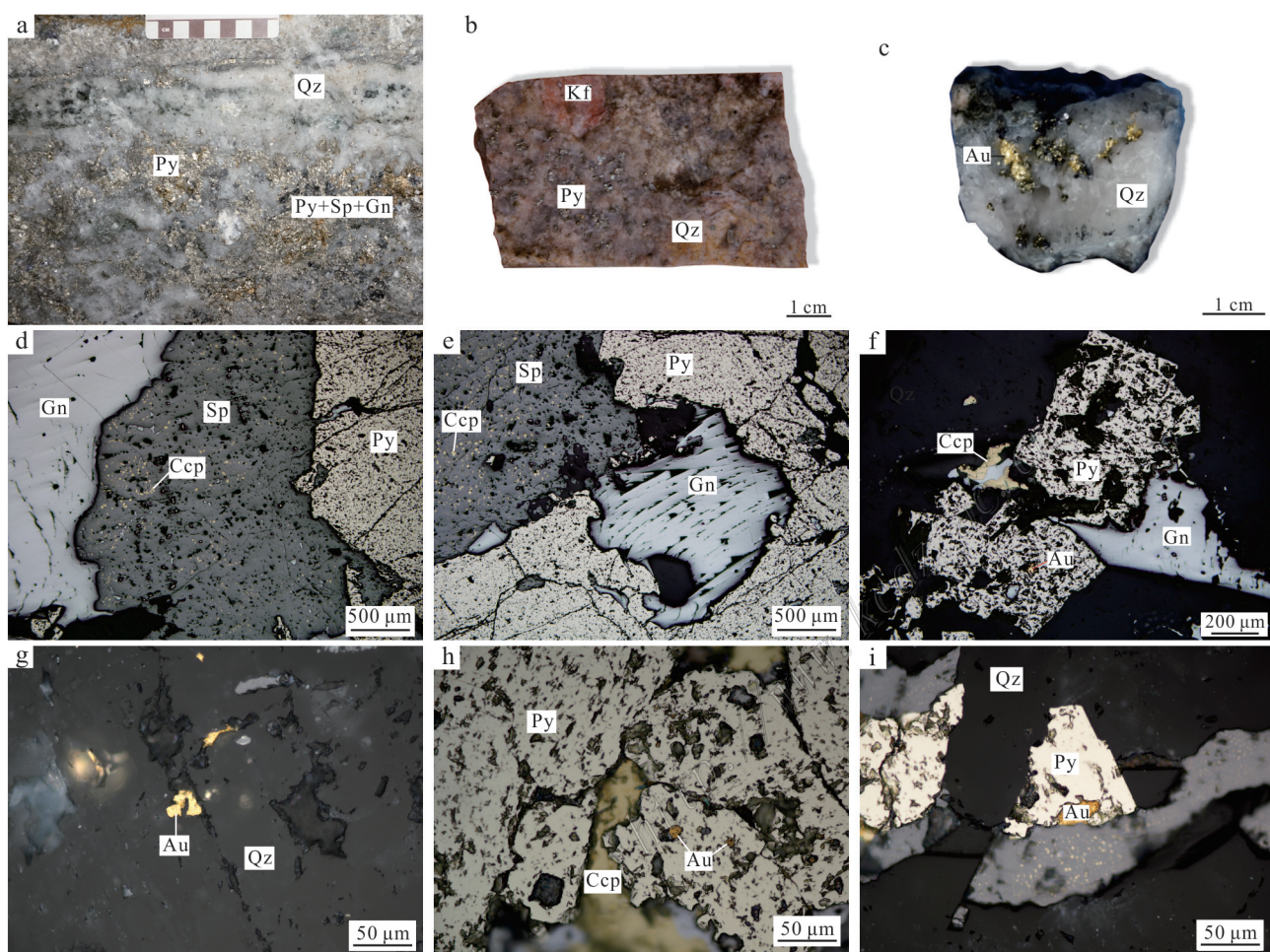


图3 石家金矿床典型矿石标本及显微照片

a.石英-硫化物脉型矿石;b.蚀变岩型矿石;c.含金石英脉型矿石;d~f.黄铁矿、闪锌矿、方铅矿、石英等矿物共生(反射光);g.石英中的包体金(反射光);h~l.黄铁矿中的包体金(反射光)

Au—自然金;Ccp—黄铜矿;Gn—方铅矿;Kf—钾长石;Py—黄铁矿;Qz—石英;Sp—闪锌矿

Fig. 3 Photographs and microphotographs of typical ore samples from the Shijia gold deposit

a. Quartz-sulfide vein type ore; b. Altered rock type ore; c. Gold-bearing quartz vein type ore; d~f. Coexistence of pyrite, sphalerite, galena and quartz (reflected light); g. Gold in quartz(reflected light); h~l. Gold in pyrite (reflected light)

Au—Native gold; Ccp—Chalcopyrite; Gn—Galena; Kf—K-feldspar; Py—Pyrite; Qz—Quartz; Sp—Sphalerite

石英、绢云母、方解石、钾长石、萤石、绿泥石等(图3d~i)。矿石典型结构有结晶、共生边、交代和固溶体出溶结构等;矿石构造则常见脉状、浸染状、角砾状、块状、梳状和晶洞状构造等。热液蚀变发育,主要包括硅化、硫化物化、绢云母化、碳酸盐化和钾长石化。

根据矿物共生组合以及脉体间的穿插关系,成矿过程可以划分为3个阶段:①石英-黄铁矿-绢云母阶段,②石英-金-多金属硫化物阶段(主成矿阶段)以及③石英-方解石-萤石阶段(Feng et al., 2020; 冯李强等,2023)。黄铁矿主要产于前两个成矿阶段。石英-黄铁矿-绢云母阶段的黄铁矿粒度粗大,呈不规

则粒状以星散状或浸染状分布于黄铁绢英岩化花岗岩之中,共生矿物主要为石英和绢云母(图4a、图4b)。在石英-金-多金属硫化物阶段,黄铁矿含量明显增加,占金属矿物的40%以上,呈自形立方体或不规则粒状,与石英、闪锌矿、方铅矿、黄铜矿以及自然金共生(图3d~i、图4c、4d)。自然金呈粒状、树枝状和不规则状,以包体金的形式赋存于石英和黄铁矿颗粒中(图3g~i)。

## 2 测试方法

用于黄铁矿热电性与晶胞参数分析的样品采自

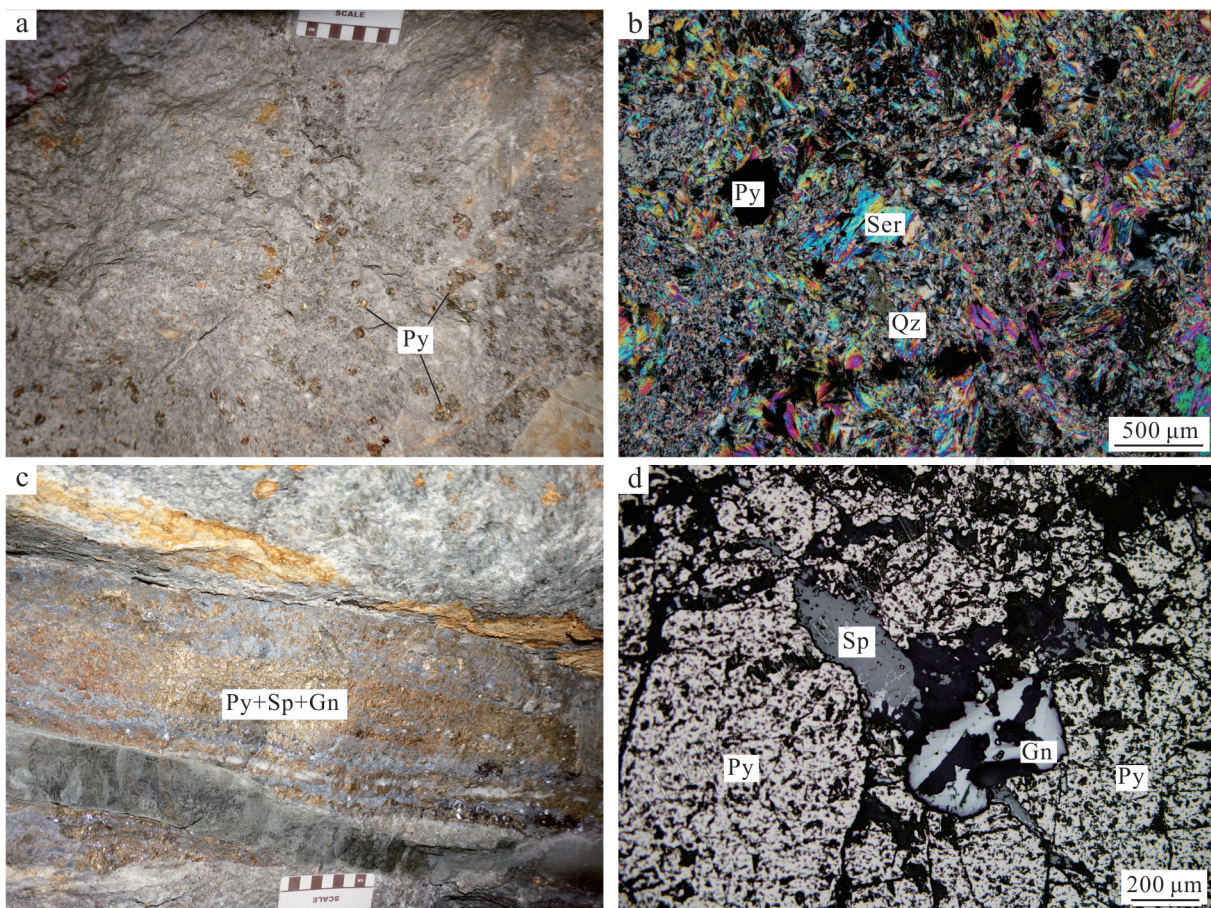


图4 石家金矿床不同矿化阶段黄铁矿特征

a. 黄铁绢英岩化花岗岩中的粗粒黄铁矿;b. 石英-黄铁矿-绢云母阶段与绢云母共生的黄铁矿(正交偏光);c. 主成矿阶段石英-硫化物脉;d. 主成矿阶段共生的黄铁矿、闪锌矿和方铅矿(反射光)

Gn—方铅矿; Py—黄铁矿; Qz—石英; Ser—绢云母; Sp—闪锌矿

Fig. 4 Characteristics of pyrite in different mineralization stages of the Shijia gold deposit

a. Coarse pyrite in pyrite sericitized (phyllitic altered) granite; b. Pyrite coexisting with sericite in the quartz-pyrite-sericite stage (cross-polarized light); c. quartz-sulfide vein of the main-ore stage; d. Pyrite, sphalerite and galena coexisting in the main-ore stage (reflected light)

Gn—Galena; Py—Pyrite; Qz—Quartz; Ser—Sericite; Sp—Sphalerite

石家金矿床326号矿脉,详细的采样位置见表1。经挑选后,共计12件石英-硫化物脉型矿石被用于挑选黄铁矿单矿物。黄铁矿热电性测试在中国地质大学(北京)成因矿物实验室完成,仪器为BHT-E-06型热电系数测量仪。测试时,冷端温度和热端温度分别为24°C和90°C,活化温度为(60±2)°C,测试前黄铁矿样品用纯酒精溶液清洗表面氧化膜和杂质。每件样品随机选取50粒以上的单矿物进行测试。

粉晶衍射(XRD)实验在包钢集团矿山研究院地质室完成,仪器为PANalytical(帕纳科)生产EMPYREAN(锐影®)X射线衍射分析仪,样品粉碎至300目后置于X射线衍射分析仪样品凹槽内进行扫描。扫描方式为连续扫描,起始角度为5.0066°,终止角度为69.9806°,步长0.013°,停留时间8.67 s。高压发生器功率为4 kW,发散狭缝类型为固定类型,狭缝DS=0.4354°,RS=0.1 mm,X光源为铜靶,测量电压/电流为40 kV/40 MA,探测器为具有二维衍射功能的PLXcel3D探测器,测角仪最小步长为0.0001°,2θ线性±0.01°,具有高分辨率。

### 3 测试结果

石家金矿床主成矿阶段12个样品的647粒黄铁矿颗粒的热电系数 $\alpha$ 变化范围为-288.3~304.9 μV/°C(表2)。热电导型以P型为主,出现率为97.5%,热电系数变化范围为130.1~304.9 μV/°C,平均263.3 μV/°C;N型黄铁矿的出现率仅为2.5%,热电系数变化于-288.3~-13.3 μV/°C,平均-132.8 μV/°C。在垂向上,P型黄铁矿的出现率呈现一定程度的波动(图5)。

黄铁矿晶胞参数见表2。黄铁矿晶胞参数 $a_0$ 值介于0.5418~0.5422 nm,平均0.5420 nm, $v_0$ 值介于0.1590~0.1594 nm<sup>3</sup>,平均0.1592 nm<sup>3</sup>,整体上略大于黄铁矿的标准晶胞参数( $a_0=0.5417$  nm, $v_0=0.1590$  nm<sup>3</sup>)。

## 4 讨论

### 4.1 黄铁矿热电性特征及其地质意义

前人对黄铁矿热电性研究表明:在高温条件下(>300°C),高价离子杂质(如Co、Ni等)容易进入黄铁矿晶格替代Fe,形成的黄铁矿为电子导型(N型),其热电系数为负值;在相对低温环境下(<300°C),低价离子杂质(如As、Sb、Te等)更易于进入黄铁矿晶格替代S,形成的黄铁矿表现为空穴导型(P型),其热电系数为正值(邵伟等,1990)。对热液矿床来说,S、As、Sb等挥发性组分通常聚集在矿体浅部,从而造成黄铁矿热电导型的分布在矿体轴向上也具有一定的规律,通常从浅至深表现出P型(浅部)→P+N型(中部)→N型的变化趋势(薛建玲等,2013)。同时,相较于N型黄铁矿,Au更倾向于被P型黄铁矿吸附(Pridmore et al., 1976),这是因为在饱和溶液中,含As的P型黄铁矿的晶格相对于游离态的黄铁矿较大,P型黄铁矿先吸附Au的络合物,导致P型黄铁矿的晶格发生畸变,并将Au<sup>+</sup>还原成Au<sup>0</sup>,进而引发Au的沉淀(Fuchs et al., 2016)。因此,当某处黄铁矿的出现率大于80%时,基本可以指示该处位于矿体的上部,并且可以作为大型矿床的指示标志(吴晋超等,2020)。

表1 石家金矿床主成矿阶段黄铁矿样品采样位置

Table 1 Location of samples of main-ore stage pyrite from the Shijia gold deposit

序号	样品编号	矿体编号	勘探线编号	采样深度/m	样品类型
1	SJ-1Py	326	28线	-595	含黄铁矿石英脉
2	SJ-2Py	326	28线	-555	含黄铁矿石英脉
3	SJ-3Py	326	28线	-515	含黄铁矿石英脉
4	SJ-4Py	326	28线	-475	含黄铁矿石英脉
5	SJ-5Py	326	28线	-435	含黄铁矿石英脉
6	SJ-6Py	326	28线	-395	多金属硫化物石英脉
7	SJ-7Py	326	28线	-355	乳白色石英-多金属硫化物脉
8	SJ-8Py	326	32线	-315	乳白色石英-多金属硫化物脉
9	SJ-9Py	326	40线	-280	乳白色石英-多金属硫化物脉
10	SJ-10Py	326	40线	-240	乳白色石英硫化物脉
11	SJ-11Py	326	52~56线之间	-205	乳白色石英硫化物脉
12	SJ-12Py	326	56线	-165	乳白色石英硫化物脉

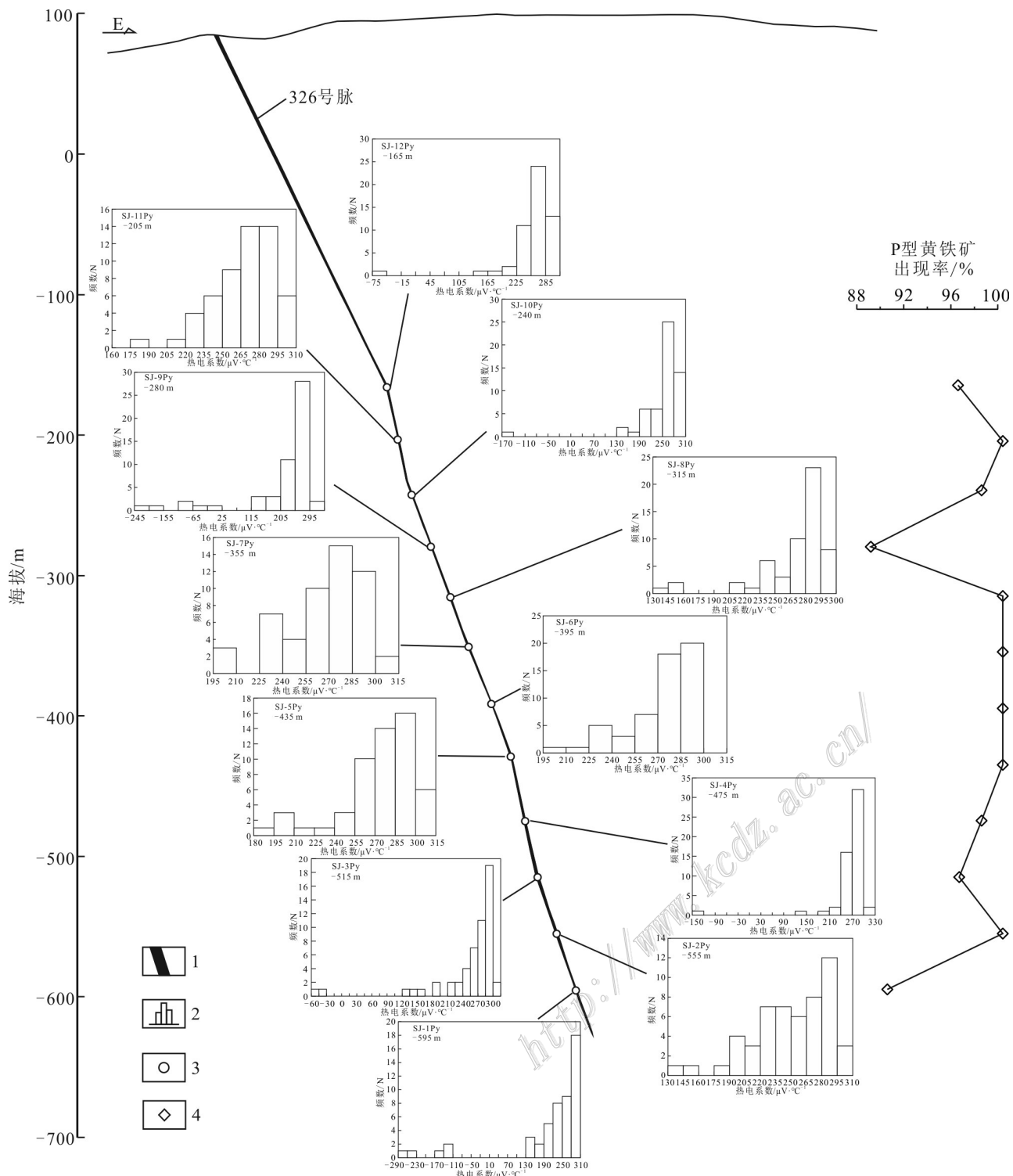


图5 石家金矿不同标高黄铁矿热电系数分布图与P型黄铁矿出现率垂向变化趋势图  
1—矿体;2—黄铁矿热电系数直方图;3—采样点;4—比率

Fig. 5 Diagram of pyrite thermoelectric coefficient at different elevations and attitude-changing trend diagram of frequency of P-type pyrite occurrence rate in the Shijia gold deposit

1—Orebody; 2—Histogram of pyrite thermoelectric coefficient; 3—Sampling location; 4—Proportion

#### 4.1.1 黄铁矿热电性的空间分布特征

石家金矿床主成矿阶段黄铁矿的热电导型整体

上以P型为主,且不同深度P型黄铁矿出现率均大于80%(88.8%~100%,表2),表明在-595 m~-165的深

表2 石家金矿床326号脉主成矿阶段黄铁矿热电系数与导型特征参数

Table 2 Thermoelectric coefficient and conductivity characteristic parameters of main-ore stage pyrite from no. 326 orebody in the Shijia gold deposit

样号	标高/m	勘探线	P型热电系数 $\alpha$ ( $\mu\text{V}/^\circ\text{C}$ )			出现率/%	温度/ $^\circ\text{C}$	N型热电系数 $\alpha$ ( $\mu\text{V}/^\circ\text{C}$ )			出现率/%	温度/ $^\circ\text{C}$	$X_{NP}$	$\gamma$ /%	$\sigma_a'$ /%
			最小值	最大值	平均值			最小值	最大值	平均值					
SJ-1Py	-595	28	137.1	296.4	244.8	90.2	156~251	-288.3	-132.2	-186.8	9.8	229~315	64	34.0	68
SJ-2Py	-555	28	132.7	299.9	249.7	100.0	153~253						89	27.8	15
SJ-3Py	-515	28	132.7	304.9	256.6	96.3	153~256	-58.8	-43.0	-50.9	3.7	355~364	83	29.2	28
SJ-4Py	-475	28	140.7	302.6	270.7	98.2	158~255		-146.1	-146.1	1.8	307	95	26.4	24
SJ-5Py	-435	28	180.9	303.5	272.6	100.0	182~255						98	25.5	10
SJ-6Py	-395	28	198.8	299.2	272.8	100.0	193~253						98	25.5	8
SJ-7Py	-355	28	195.8	302.4	266.0	100.0	191~255						96	25.9	10
SJ-8Py	-315	32	130.1	304.0	268.8	100.0	151~256						95	26.3	14
SJ-9Py	-280	40	137.8	300.6	252.2	88.8	156~254	-241.0	-13.3	-114.2	11.8	255~380	70	32.6	60
SJ-10Py	-240	40	130.9	295.7	255.3	98.2	152~251		-180.5	-180.5	1.8	288	87	28.2	28
SJ-11Py	-205	52~56	184.1	298.1	267.0	100.0	184~252						98	25.5	10
SJ-12Py	-165	56	173.5	300.8	264.5	96.2	156~254		-77.6	-77.6	3.8	345	92	26.9	22

注: $\alpha$ 为热电系数, $X_{NP}$ 为热电性参数, $\gamma$ 为剥蚀率, $\sigma_a'$ 为热电系数离散度。

度范围内仍处于矿化系统的上部或者中上部位置,因此推测-595 m以下仍具有较好的找矿前景。此外,P型黄铁矿出现率在垂向上出现一定的波动(图5),这反映成矿过程经历了多次地质热事件,可能存在叠加成矿或多期次成矿。

黄铁矿热电系数离散范围(也即热电系数的变化区间)也可以反映矿化的强弱。当离散范围较大时,矿化较强,矿体规模较大,矿石的品位也可能较高(李青等,2013),例如石湖、义兴寨、金青顶等大型-特大型石英脉型金矿床黄铁矿热电系数变化范围分别为-293~306  $\mu\text{V}/^\circ\text{C}$ (曹烨等,2008)、-350~350  $\mu\text{V}/^\circ\text{C}$ (李成禄等,2009)、-530~496  $\mu\text{V}/^\circ\text{C}$ (陈海燕等,2010)。石家金矿黄铁矿热电系数 $\alpha$ 变化于-288.3~304.9  $\mu\text{V}/^\circ\text{C}$ ,与同属大柳行地区的黑岚沟、河西、齐沟等金矿床中黄铁矿 $\alpha$ 值的变化范围一致(图6)。较大的热电系数离散范围指示矿区深部仍具有较强矿化和良好的成矿潜力。

#### 4.1.2 黄铁矿热电系数离散度

黄铁矿热电系数离散度( $\sigma_a'$ )可以准确地反映不同样品的热电系数的集中与分散情况(邵伟等,1990;刘平等,1991;杨竹森等,2000),其计算公式为: $\sigma_a' = \sigma_a/\alpha' \times 100\%$ ,式中, $\alpha'$ 为黄铁矿样品热电系数的平均值, $\sigma_a$ 为热电系数的标准差。热电系数离散度可以反映成矿条件的稳定程度,即在较稳定的成矿条件下形成的黄铁矿晶体性质接近,热电系数离散范围较小,则 $\sigma_a'$ 值也相应较小;反之,波动范围

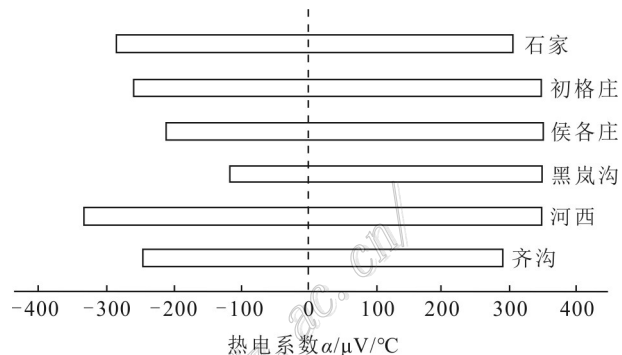


图6 大柳行地区金矿床黄铁矿热电系数离散范围图(底图  
据吴晋超等,2021)

Fig. 6 Discrete range of thermoelectric coefficient of pyrite from gold deposits in the Daliuhang area (base map after Wu et al., 2021)

较大, $\sigma_a'$ 值较大(刘冲昊等,2013)。热点系数离散度与P型黄铁矿的出现率也可以指示矿化程度。当P型黄铁矿出现率高且对应的 $\sigma_a'$ 值较小时,矿化程度较好;当P型黄铁矿出现率高且对应的 $\sigma_a'$ 值较大时,矿化不连续;当P型黄铁矿出现率低且 $\sigma_a'$ 值偏大时,矿化程度较差(张方方等,2013;刘坤等,2014;刘华南等,2018)。

石家主成矿阶段黄铁矿热电系数离散度为8%~68%,主要集中于10%~30%(表2,图7a),指示黄铁矿整体形成于较为稳定的条件下。同时,在P型黄铁矿出现率与离散度关系图中,出现率与离散度呈

一定的负相关关系,在-435~315 m标高范围内,高的P型黄铁矿出现率与低的 $\sigma_a'$ 值相对应(图7b),表明该段矿体矿化程度较好。在矿区南部矿石品位等值线图中,该标高范围内的样品(28线)基本上处于等值线图中高品位区域内(图8),支持了该段矿体矿化程度较好这一结论。

#### 4.1.3 矿体剥蚀程度

根据热电系数可以计算出黄铁矿的热电性参数( $X_{NP}$ ),进而可以获得矿体的剥蚀率( $\gamma$ )。黄铁矿的热电性参数 $X_{NP}=(2f_I+f_{II})-(f_{IV}+2f_V)$ ,式中, $f$ 为样品中相应热电系数值域的黄铁矿百分比, $f_I$ 为 $\alpha>400 \mu\text{V}/\text{C}$ , $f_{II}$ 为 $\alpha=200\sim400 \mu\text{V}/\text{C}$ , $f_{IV}$ 为 $\alpha=0\sim200 \mu\text{V}/\text{C}$ , $f_V$ 为 $\alpha<-200 \mu\text{V}/\text{C}$ ,矿体剥蚀程度 $\gamma=50-X_{NP}/4$ (权志高,1995)。根据以上公式得到黄铁矿热电性参数为64~98,石家金矿326号脉剥蚀率为25.5%~34.0%,较低的剥蚀率表明矿体保存较为完好,矿区深部具有较好的找矿前景,这与P型黄铁矿出现率所指示的-595~-165 m的深度仍处在矿体上部或中上部的结论一致。此外,黑岗沟金矿田在-616~-170 m区间内矿体的剥蚀率为25.0%~40.5%,平均为30.4%(吴晋超等,2021),推测大柳行地区矿体剥蚀程度整体较低,在-600 m以下找矿潜力良好,有寻找大型金矿床的可能。

#### 4.1.4 黄铁矿形成温度

黄铁矿的热电系数和热电导型与其形成温度具有密切联系,可以作为地质温度计用于判别成矿温度(Wang et al., 2016; Alam et al., 2019)。两种不同

导型黄铁矿的形成温度与热电系数之间的关系式分别为(薛建玲等,2013; Wang et al., 2016):

$$T(\text{°C})=3\times(122.22+\alpha)/5.0 (\text{P型})$$

$$T(\text{°C})=(704.51-|\alpha|)/1.818 (\text{N型})$$

根据上述公式计算得到石家金矿床中P型黄铁矿的结晶温度为151~256°C,N型黄铁矿形成温度介于229~380°C,表明黄铁矿的结晶温度为151~380°C,这一温度范围与大柳行地区金矿床石英中流体包裹体的显微测温结果一致(160~390°C;马顺溪等,2020;于晓卫等,2023)。由黄铁矿热电系数-温度图(图9a)和温度直方图(图9b)可知,石家金矿床黄铁矿形成温度集中于210~250°C,与大柳行地区黑岗沟等其他金矿床的形成温度基本一致(集中于200~280°C;吴晋超等2021),表明石家金矿床形成于中温条件下。由于叠加成矿或者多期次成矿,高温条件下形成的N型黄铁矿与低温环境下结晶的P型黄铁矿在空间位置上相互重叠,从而导致由相同采样位置的2种类型黄铁矿所计算的温度存在较大差异。

#### 4.2 黄铁矿晶胞参数及其地质意义

黄铁矿晶胞参数对于金矿勘查具有标型意义,越是偏离标准值的黄铁矿,其含金性越好(贾建业,1996)。黄铁矿晶胞参数变化原因目前有2种解释:  
①当Co、Ni、As、Sb、Te等微量元素以类质同象形式进入黄铁矿晶格置换Fe或者S时(Abraitis et al., 2004),会导致晶胞参数 $a_0$ 变大;  
②当S离子亏损,S/Fe<2时,黄铁矿S空位的形成导致Fe-S共价键增加,Fe-S键长减小,致使黄铁矿晶胞参数 $a_0$ 变小(曹烨

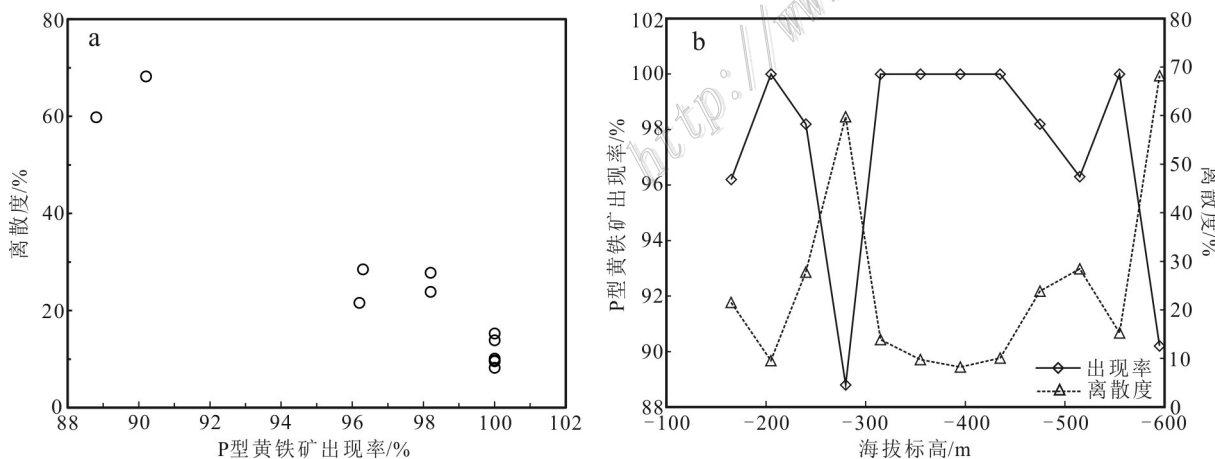


图7 石家金矿床P型黄铁矿出现率与热点系数离散度关系图(a)以及出现率、离散度与标高关系图(b)

Fig. 7 Relationship between occurrence rate and thermoelectrical coefficient dispersion of P-type pyrite (a) and relationship among occurrence rate, thermoelectrical coefficient dispersions and elevation (b) from the Shijia gold deposit

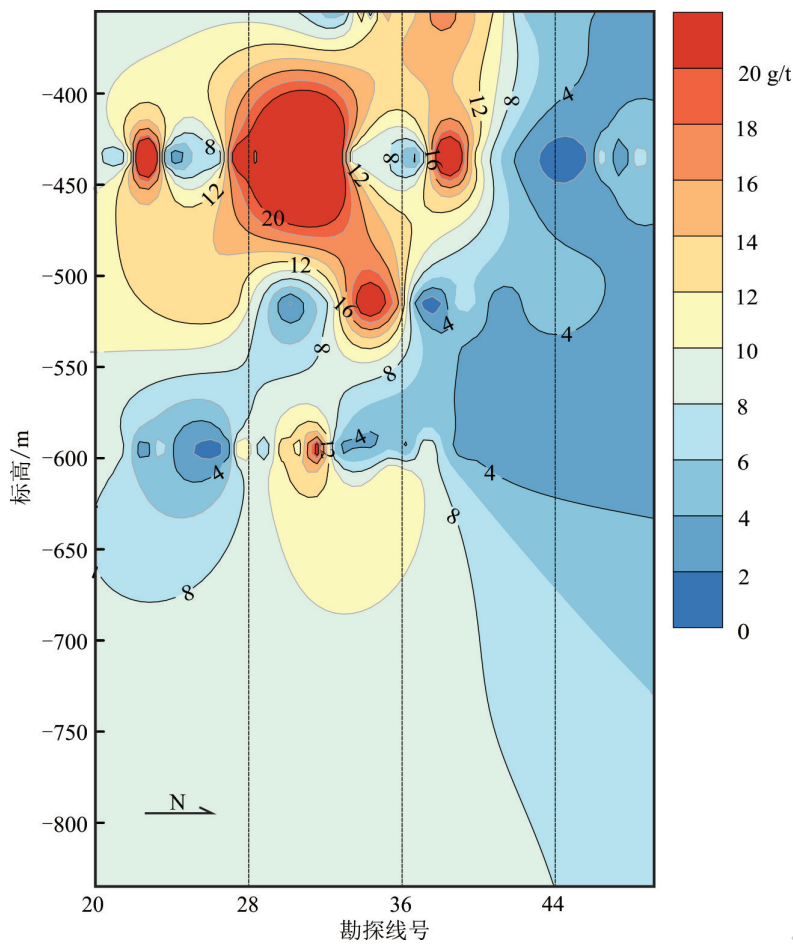


图8 石家金矿区南部矿石品位等值线图(据山东省第六地质矿产勘查院资料整理)

Fig. 8 Contour map of gold ore grade in the southern part of the Shijia gold deposit(data from the Sixth Geological and Mineral Exploration Institute of Shandong Province)

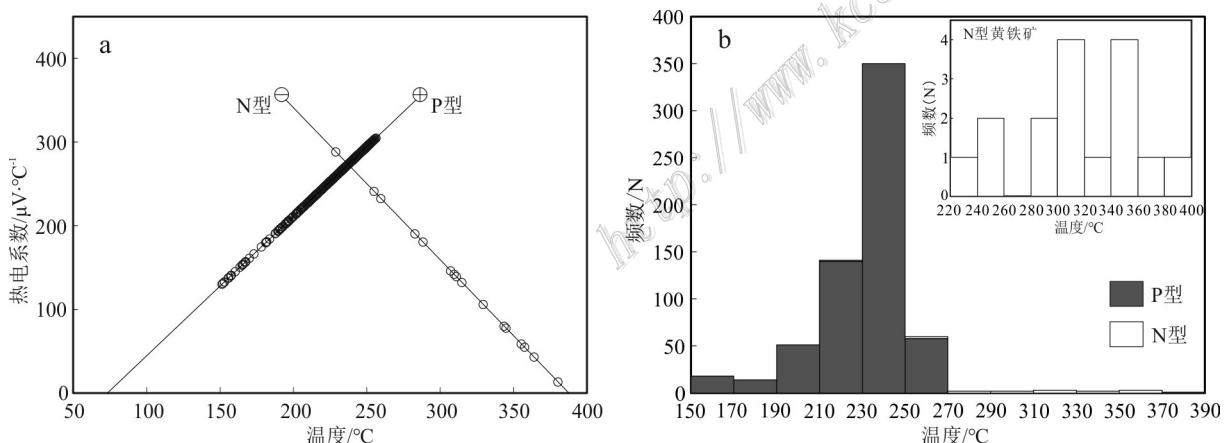


图9 石家金矿床黄铁矿热电系数-温度图解(a)与温度直方图(b)

Fig. 9 The relationship between thermoelectricity and temperature(a) and tempreture histogram(b) of pyrite from the Shijia gold deposit

等,2010)。

石家金矿床主成矿阶段黄铁矿的晶胞参数 $a_0$ 值

介于0.5418~0.5422 nm(表3),略大于黄铁矿的标准晶胞参数( $a_0=0.54176$  nm),与胶东地区邓各庄、金

表3 石家金矿床主成矿阶段黄铁矿晶胞参数  
Table 3 Cell parameters of main-ore stage pyrite from no. 326 orebody in the Shijia gold deposit

样号	标高/m	$a_0/\text{nm}$	$v_0/\text{nm}^3$	$\Delta a/\text{nm}$	$w(\text{Co}+\text{Ni})/10^{-6}$
SJ-1Py	-595	0.5420	0.1592	0.0003	176.9
SJ-2Py	-555	0.5420	0.1592	0.0003	90.7
SJ-3Py	-515	0.5418	0.1590	0.0001	31.5
SJ-4Py	-475	0.5422	0.1594	0.0005	10.3
SJ-5Py	-435	0.5420	0.1592	0.0003	6.0
SJ-6Py	-395	0.5418	0.1590	0.0001	4.2
SJ-7Py	-355	0.5418	0.1590	0.0001	18.3
SJ-8Py	-315	0.5421	0.1593	0.0004	198.8
SJ-9Py	-280	0.5418	0.1590	0.0001	42.1
SJ-10Py	-240	0.5422	0.1594	0.0005	56.7
SJ-11Py	-205	0.5421	0.1593	0.0004	116.5
SJ-12Py	-165	0.5420	0.1592	0.0003	88.4

注: $w(\text{Co}+\text{Ni})$ 据冯李强等(2023)。

青顶等石英脉型金矿床的晶胞参数近于一致(图10)。晶胞参数变大,表明Co、Ni、As等元素进入黄铁矿晶格置换了Fe或者S。以下证据表明石家金矿床黄铁矿晶胞参数变大更可能与As进入黄铁矿晶格替代S有关:①石家金矿床中黄铁矿的热电导型以P型为主,并且黄铁矿的 $w(\text{Co}+\text{Ni})$ 整体较低( $4.2 \times 10^{-6} \sim 198.8 \times 10^{-6}$ ,表3);②在原生晕纵剖面图上采样点均位于As的内带异常范围内( $w(\text{As}) \geq 224.8 \times 10^{-6}$ ;张英帅等,2021);③同区域黑岚沟金矿床中主成矿阶段黄铁矿显示出富集As元素的特征(Feng et al., 2018;李秀章等,2022)。由于As的离子半径大于S,当As以类质同象替换S进入黄铁矿形成As-S共价键,导致黄铁矿晶格发生畸变并出现晶格缺陷,从而有利于Au进入黄铁矿晶格(刘一浩等,2020;孙宁岳等,2022)。黑岚沟金矿床黄铁矿中Au与As表现出极强的正相关性,证实了黄铁矿内存在晶格金( $\text{Au}^+$ )和显微包裹金( $\text{Au}^0$ )等不可见金(Feng et al., 2018;李秀章等,2022)。因此,黄铁矿中As的富集可能是导致Au沉淀的重要因素。石家金矿床黄铁矿的晶胞参数整体上大于标准值,并且晶胞参数变化主要与As的富集有关,因而推测在-595~ -165 m范围内,矿化程度较好。

## 5 结 论

(1) 石家金矿床主成矿阶段黄铁矿热电导型以

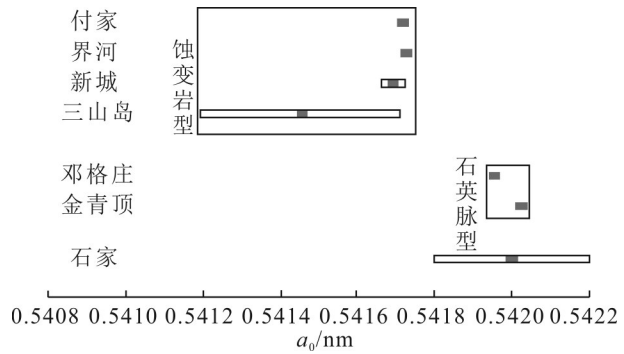


图10 胶东地区各金矿床多金属硫化物阶段黄铁矿晶胞参数图(底图据张龙等,2020)

Fig. 10 Cell parameters of pyrite in polymetallic sulfide stage of gold deposits in Jiaodong area (base map after Zhang et al., 2020)

P型为主,热电系数具有较大离散范围,同时矿体剥蚀率为25.5%~34.0%,表明目前探采部位仍处于矿化系统上部,深部具有良好的找矿前景。

(2) 黄铁矿热电系数离散度整体较小,反映黄铁矿的形成条件相对稳定。根据热电系数计算黄铁矿的形成温度集中于210~250°C,表明石家金矿床为中温矿床。

(3) As等元素的类质同象替换黄铁矿晶格中的S是导致石家金矿床黄铁矿晶胞参数变大的主要因素,黄铁矿的晶胞参数可作为重要的找矿标志。

**致 谢** 研究工作得到了中国地质大学(北京)王佳琳博士、葛战林博士、何宇硕士的帮助,野外工作得到了山东蓬莱万泰矿业有限公司李思野、赵刘雍等相关工作人员的大力支持,两位匿名审稿专家提出了宝贵的修改意见,在此一并致以诚挚的感谢!

## References

- Abratis P K, Patrick R A D and Vaughan D J. 2004. Variations in the compositional, textural and electrical properties of natural pyrite: A review[J]. International Journal of Mineral Processing, 74(1-4): 41-59.
- Alam M, Li S R, Santosh M, Shah A, Yuan W M, Khan H, Quaeshi J A and Zeng Y J. 2019. Morphological, thermoelectrical, geochemical and isotopic anatomy of auriferous pyrite from the Bagrote valley placer deposits, North Pakistan: Implications for ore genesis and gold exploration[J]. Ore Geology Reviews, 112: 103008.
- Cao Y, Li S R, Ao C, Li Z Z and Liu X B. 2008. Application of thermo-

- electric properties of pyrite in gold exploration in the Shihu gold deposit, western Hebei[J]. *Geology in China*, 35(4): 746-753(in Chinese with English abstract).
- Cao Y, Li S R, Zhang H F, Ao C, Li Z Z and Liu X B. 2010. Characteristics of cell parameters of pyrite and quartz and their geological significance at Shihu gold deposit in western Hebei, North China[J]. *Bulletin of Mineralogy, Petrology and Geochemistry*, 29(2): 185-191(in Chinese with English abstract).
- Chen H Y, Li S R, Zhang B, Zhou Q F, Zhang Y Q, Liu Z H, Zhang H F and Wang N. 2010. Thermoelectric character of pyrite from Jin-qingding glod deposit in eastern Shandong Province and its significance[J]. *Mineral Deposits*, 29(6): 1125-1137(in Chinese with English abstract).
- Fan H R, Feng K, Li X H, Hu F F and Yang K F. 2016. Mesozoic gold mineralization in the Jiaodong and Korean Peninsula[J]. *Acta Petrological Sinica*, 32(1): 3225-3258(in Chinese with English abstract).
- Feng L Q, Gu X X, Zhang Y M, Wang J L, Ge Z L, He Y and Zhang Y S. 2020. Geology and geochronology of the Shijia gold deposit, Jiaodong Peninsula, China[J]. *Ore Geology Reviews*, 120: 103432.
- Feng L Q, Gu X X, Zhang Y M, Zhang Y S, Wang P F, Yan H W and Wang D W. 2023. Trace element geochemical characteristics of gold-bearing pyrite from the Shijia gold deposit in Penglai, Shandong Province and its constraints on ore-forming fluids[J]. *Northwestern Geology*, 56(5): 262-277(in Chinese with English abstract).
- Feng K, Fan H R, Hu F F, Yang K F, Liu X, Shangguan Y N, Cai Y C and Jiang P. 2018. Involvement of anomalously As-Au-rich fluids in the mineralization of the Heilan' gou gold deposit, Jiaodong, China: Evidence from trace element mapping and in-situ sulfur isotope composition[J]. *Journal of Asian Earth Sciences*, 160: 304-321.
- Fuchs S, William-Jones A E and Przybylowicz W J. 2016. The origin of the gold and uranium ores of the Black Reef Formation, Transvaal Supergroup, South Africa[J]. *Ore Geology Reviews*, 72: 149-164.
- Gao Y W, Wang Z H, Li W L and Zhang Z L. 2019. A review of pyrite mineralogy research in hydrothermal gold deposit[J]. *Northwestern Geology*, 52(3): 58-69(in Chinese with English abstract).
- Gu X X, Li B H, Zhang Y M, Peng Y W and Xiang Z L. 2019. Methods and applications of ore deposit study[M]. Beijing: Geological Publishing House. 1-815(in Chinses).
- Jia J Y. 1996. X-ray diffraction spectrum of pyrite and its prospecting significance[J]. *Northwestern Geology*, 17(3): 38-45(in Chinese).
- Li C L, Li S R, Luo J Y, Song J X and Zhang J Q. 2009. Thermoelectric coefficient, conductive type and significance of the pyrite from Yixingzhai gold deposit in Fanshi County, Shanxi Province, China[J]. *Geoscience*, 23(6): 1056-1063(in Chinses with English abstract).
- Li Q, Li S R, Zhang X B, Zhang L J, Zhao Y, Zhao F W and Liu Y. 2013. Thermoelectric coefficient of pyrite from the Xishimen gold deposit in Lingshou County, Hebei Province and its prospecting significance[J]. *Acta Geologica Sinica*, 87(4): 542-553(in Chinese with English abstract).
- Li X H, Fan H R, Hu F F, Hollings P, Yang K F and Liu X. 2019. Linking lithospheric thinning and magmatic evolution of Late Jurassic to Early Cretaceous granitoids in the Jiaobei Terrane, southeastern North China Craton[J]. *Lithos*, 324-325: 280-296.
- Li X Z, Wang Y J, Li Y X, Fu L B, Zhang M, Wu X Y, Zhao Y Y, Huang X, Xu C and Kong F S. 2022. Micro-geochemical characteristic of pyrites in the Heilangou gold deposit of penglai area and its implications for ore-forming fluid, Jiaodong gold Province[J]. *Geological Bulletin of China*, 41(6): 1023-1038(in Chinese with English abstract).
- Liu C H, Liu J J, Wang J P, Wu J, Wang W Y, Wang L X, Chen D and Li Z G. 2013. Thermoelectric characteristics of pyrite from the main one zone of the Huachanggou gold deposit, Shaanxi Province[J]. *Earth Science Frontiers*, 20(4): 264-272(in Chinses with English abstract).
- Liu H N, Liu J J, Li X W, Liu C H, Dai H Z, Tao Y L, Wang J F, Du Y D and Fan Y F. 2018. Thermoelectric characteristics of pyrite from the Xindigou gold deposit in Inner Mongolia and its significance on deep prospecting[J]. *Geology in China*, 45(4): 819-838 (in Chinese with English abstract).
- Liu K, Liu J J, Wu J, Liu C H, Yang S S, Xin X J and Li Y. 2014. Thermoelectric characteristic of pyrites from No.8 orebody of the Mawu gold deposit in Gansu Province and its significance[J]. *Geoscience*, 28(4): 711-720(in Chinese with English abstract).
- Liu P and Qiu Z X. 1991. The distribution features of pyroelectric coefficient values of pyrite samples from some gold deposits in China and their significance[J]. *Acta Mineralogica Sinica*, 11(1): 60-69 (in Chinese with English abstract).
- Liu Y H, Xue C J, Zhao Y, Zhao X B, Chu H X, Liu C X, Yu L, Wang L and Wu D H. 2020. Research on auriferous pyrite in hydrothermal gold deposits, China[J]. *Geoscience*, 34(1): 1-12(in Chinese with English abstract).
- Ma L, Jiang S Y, Dai B Z, Jiang Y H, Hou M L, Pu W and Xu B. 2013. Multiple sources for the origin of Late Jurassic Linglong adakitic granite in the Shandong Peninsula, eastern China: Zircon U-Pb geochronological, geochemical and Sr-Nd-Hf isotopic evidence[J]. *Lithos*, 162-163: 251-263.
- Ma S X, Bai Y N, Sun Y L and Shu J D. 2020. Fluid inclusions and stable isotopes study of Yanshan gold deposit in the Penglai area, eastern Shandong Provinc[J]. *Acta Geologica Sinica*, 94(11): 3391-3403(in Chinese with English abstract).
- Pridmore D F and Shuey R T. 1976. The electrical resistivity of galena, pyrite, and chalcopyrite[J]. *American Mineralogist*, 61(3-4): 248-259.
- Quan Z G. 1995. A study on thermoelectricity of gold-bearing pyrite in Pangjiahe and Zuojiazhuang deposits[J]. *Mineral Resources and Geology*, 9(6): 509-513(in Chinese with English abstract).
- Shao W, Chen G Y and Sun D S. 1991. Method of investigating ther-

- moelectricity of pyrite and its application to pyrites from gold deposits in Jiaodong region[J]. Geoscience, 4(1): 46-57(in Chinese with English abstract).
- Shen J F, Liu S R, Ma G G, Liu Y, Yu H J and Liu H M. 2013. Typomorphic characteristics of pyrite from the Linglong gold deposit: Its vertical variation and prospecting significance[J]. Earth Science Frontiers, 20(3): 55-75(in Chinese with English abstract).
- Shen J F, Li S R, Huang S F, Qing M, Zhang H F and Xu B. 2021. The decennary new advances on the genetic mineralogy and prospecting mineralogy (2010-2020)[J]. Bulletin of Mineralogy, Petrology and Geochemistry, 40(3): 610-623.
- Shi Q H, Zhang Y M, Gu X X, Feng L Q, Wang J L, Zhang Y S. 2023. Geochemical characteristics and petrogenesis of the Early Cretaceous mafic-felsic dykes in the Shijia gold deposit, Penglai, Shandong Province[J]. Northwestern Geology, 56(1): 99-116(in Chinese with English abstract).
- Song M C, Lin S Y, Yang LQ, Song Y X, Ding Z J, Li Jie, Li S Y and Zhou M L. 2020. Metallogenetic model of Jiaodong Peninsula gold deposits[J]. Mineral Deposits, 39(2): 215-236(in Chinese with English abstract).
- Sun N Y, Li G W, Shen J F, Gao J W and Xue Y. 2022. Relationship between fine structure and cell parameters of pyrite and their typomorphic significance[J]. Northwestern Geology, 55(4): 333-342 (in Chinese with English abstract).
- Wang G W, Feng Y, Carranza E J M, Li R X, Li Z L, Feng Z K, Zhao X D, Wang D J, Kong L, Jia W J and Wen B T. 2016. Typomorphic characteristics of pyrite: Criteria for 3D exploration targeting in the Xishan gold deposit, China[J]. Journal of Geochemical Exploration, 164: 136-163.
- Wu J C, Shen J F, Li G W, Li S R, He Z Y, Du B S, Xu K X, Qiu H C and Li J P. 2020. The improved method for measuring thermoelectric property of pyrite and its implication for exploring gold resources—a case study of the Wulong gold deposit in Liaoning Province[J]. Bulletin of Mineralogy, Petrology and Geochemistry, 39(2): 283-292(in Chinese with English abstract).
- Wu J C, Shen J F, Shen Y K, Li G W, Zhang H F, Du B S, He Z Y and Xu K X. 2021. The rmoelectricity property and deep metallogenetic forecast of pyrite in Heilangou gold field of Jiaodong, Shandong Province[J]. Northwestern Geology, 54(2): 111-124(in Chinese with English abstract).
- Xue J L, Li S S, Sun W Y, Zhang Y Q and Zhang X. 2013. Characteristics of the genetic mineralogy of pyrite and its significance for prospecting in the Denggezhuang gold deposit, Jiaodong Peninsula, China[J]. Science China: Earth Sciences, 43(11): 1857-1873(in Chinese with English abstract).
- Yang K F, Fan H R, Santosh M, Hu F F, Wilde S A, Lan T G, Lu L N and Liu Y S. 2012. Reactivation of the Archean lower crust: Implications for zircon geochronology, elemental and Sr-Nd-Hf isotopic geochemistry of late Mesozoic granitoids from northwestern Jiaodong Terrane, the North China Craton[J]. Lithos, 146-147: 112-127.
- Yang Q Y, Santosh M, Shen J F and Li S R. 2014. Juvenile vs. recycled crust in NE China: Zircon U-Pb geochronology, Hf isotope and an integrated model for Mesozoic gold mineralization in the Jiaodong Peninsula[J]. Gondwana Research, 25: 1445-1468.
- Yang Z S, Li H Y, Gao Z M and Wang Z J. 2000. A study on thermoelectricity of pyrite from superhigh-grade gold deposits, northern Jiaodong[J]. Geoscience, 19(4): 307-314(in Chinese with English abstract).
- Yu X W, Zhang W, Liu H D, Wang L M, Wang Q Y, Tian R C, Dai G K, Wang Y P, Wang J H and Chen W T. 2023. Metallogenetic fluid and material source of Ankou gold deposit in Daluhang gold ore field, Jiaodong[J]. Mineral Deposit, 42(2): 310-330(in Chinese with English abstract).
- Zhang F F, Wang J P, Liu C H, Cao R R, Cheng J J, Yang Y R, Qi F and Wang L. 2013. The crystal forms and thermoelectricity of pyrite from the Shuangwang gold deposit, Shaanxi Province and their applications to metallogenetic prognosis[J]. China Geology, 40 (5): 1633-1643(in Chinses with English abstract).
- Zhang L, Li S R, Song Y X and Zhu S Z. Typomorphic characteristics of pyrite in the Wang'ershan gold deposit, Northwest Jiaodong, and its prospecting significance[J]. Acta Peterologica et Mineralogica, 39(2): 159-171(in Chinses with English abstract).
- Zhang Y S, Gu X X, Zhang Y M, Wang J L, Feng L Q, Ge Z L and He Y. 2021. Geochemical characteristics of primary halos and deep prospecting prediction of the Shijia gold deposit in Penglai, Shandong Province[J]. Geoscience, 35(1): 258-269(in Chinses with English abstract).
- 附中文参考文献**
- 曹烨,李胜荣,敖翀,张华峰,李真真,刘小滨. 2008. 黄铁矿热电性特征在冀西石湖金矿床中的应用[J]. 中国地质,35(4):746-753.
- 曹烨,李胜荣,张华峰,敖翀,李真真,刘小滨. 2010. 冀西石湖金矿黄铁矿和石英的晶胞参数特征及其地质意义[J]. 矿物岩石地球化学通报,29(2):185-191.
- 陈海燕,李胜荣,张秀宝,周起凤,张运强,刘振豪,张海芳,王宁. 2010. 胶东金青顶金矿床黄铁矿热电性标型特征及其地质意义[J]. 矿床地质,29(6):1125-1137.
- 范宏瑞,冯凯,李兴辉,胡芳芳,杨奎锋. 2016. 胶东-朝鲜半岛中生代金成矿作用[J]. 岩石学报,32(10):3225-3238.
- 冯李强,顾雪祥,章永梅,张英帅,王鹏飞,颜宏伟,王大伟. 2023. 山东蓬莱石家金矿床含金黄铁矿微量元素地球化学特征及其对成矿流体的约束[J]. 西北地质,56(5): 262-277.
- 高永伟,王志华,黎卫亮,张振亮. 2019. 热液型金矿床中的黄铁矿矿物学研究综述[J]. 西北地质,52(3):58-69.
- 顾雪祥,李葆华,章永梅,彭义伟,向中林. 2019. 矿床学研究方法及应用[M]. 北京:地质出版社. 1-815.
- 贾建业. 1996. 黄铁矿的x射线衍射谱及其找矿意义[J]. 西北地质, 17(3):38-45.
- 李成禄,李胜荣,罗军燕,宋继叶,张聚全. 2009. 山西繁峙义兴寨金

- 矿黄铁矿热电系数与导型特征及其地质意义[J].现代地质,23(6):1056-1063.
- 李青,李胜荣,张秀宝,张林杰,赵毅,赵夫旺,刘洋.2013.河北省灵寿县西石门金矿黄铁矿热电性标型及其找矿意义[J].地质学报,87(4):542-553.
- 李秀章,王勇军,李衣鑫,付乐兵,张铭,吴兴宇,赵岩岩,黄鑫,徐昌,孔凡顺.2022.胶东蓬莱黑岚沟金矿床黄铁矿微区地球化学特征及对成矿流体的启示[J].地质通报,41(6):1023-1038.
- 刘冲昊,刘家军,王建平,吴杰,王维钰,王立新,于康伟,陈冬,李志国.2013.陕西省铧厂沟金矿床主矿带黄铁矿热电性特征及其地质意义[J].地学前缘,20(4):264-272.
- 刘华南,刘家军,李小伟,李小伟,刘冲昊,代鸿章,陶银龙,王建锋,杜映东,范云飞.2018.内蒙古新地沟金矿床黄铁矿热电性特征及深部找矿意义[J].中国地质,45(4):819-838.
- 刘坤,刘家军,吴杰,刘冲昊,杨尚松,辛晓军,李渊.2014.甘肃马坞金矿床8号矿体黄铁矿热电性特征及其地质意义[J].现代地质,28(4):711-720.
- 刘平,邱朝霞.1991.某些金矿床中黄铁矿热电系数值的分布特点及其意义[J].矿物学报,11(1):60-69.
- 刘一浩,薛春纪,赵云,赵晓波,褚海霞,刘城先,余亮,王璐,吴得海.2020.我国热液金矿中黄铁矿的载金性研究[J].现代地质,34(1):1-12.
- 马顺溪,白宜娜,孙永联,舒记德.2020.胶东蓬莱大柳行金矿田燕山金矿床流体包裹体特征和氢-氧同位素研究[J].地质学报,94(11):3391-3403.
- 权志高.1995.庞家河、左家庄金矿床载金矿物黄铁矿热电性的研究[J].矿产与地质,9(6):509-513.
- 邵伟,陈光远,孙岱生.1990.黄铁矿热电性研究方法及其在胶东金矿的应用[J].现代地质,4(1):46-56.
- 申俊峰,李胜荣,马广钢,刘艳,于洪军,刘海明.2013.玲珑金矿黄铁矿标型特征及其大纵深变化规律与找矿意义[J].地学前缘,20(3):55-75.
- 申俊峰,李胜荣,黄绍锋,卿敏,张华锋,许博.2021.成因矿物学与找矿矿物学研究进展(2010-2020)[J].矿物岩石地球化学通报,40(3):610-623.
- 石启慧,章永梅,顾雪祥,冯李强,王佳琳,张英帅.2023.山东蓬莱石家金矿床早白垩世镁铁质-长英质脉岩地球化学特征及其成因[J].西北地质,56(1):99-116.
- 宋明春,林少一,杨立强,宋英昕,丁正江,李杰,李世勇,周明岭.2020.胶东金矿成矿模式[J].矿床地质,39(2):215-236.
- 孙宁岳,李国武,申俊峰,高建伟,薛源.2022.黄铁矿精细结构与晶胞参数的关系及其标型意义[J].西北地质,55(4):333-342.
- 吴晋超,申俊峰,李国武,李胜荣,何泽宇,杜伯松,徐渴鑫,邱海城,李建平.2020.黄铁矿热电性测试方法改进及其在金矿找矿勘查中的应用——以辽宁五龙金矿为例[J].矿物岩石地球化学通报,39(2):283-292.
- 吴晋超,申俊峰,申玉科,李国武,张华峰,杜柏松,何泽宇,徐渴鑫.2021.胶东黑岚沟金矿田黄铁矿热电性研究及深部成矿预测[J].西北地质,54(2):111-125.
- 薛建玲,李胜荣,孙文燕,张运强,张旭.2013.胶东邓格庄金矿黄铁矿成因矿物学特征及其找矿意义[J].中国科学:地球科学,43(11):1857-1873.
- 杨竹森,李红阳,高振敏,王志敬.2000.胶东北部超高品质金矿黄铁矿热电性研究[J].现代地质,19(4):307-314.
- 于晓卫,张文,刘汉栋,王来明,王巧云,田瑞聪,戴广凯,王英鹏,王金辉,陈文韬.2023.胶东大柳行金矿田庵口金矿床成矿流体与成矿物质来源[J].矿床地质,42(2):310-330.
- 张方方,王建平,刘冲昊,曹瑞荣,程建军,杨永荣,齐峰,王罗.2013.陕西双王金矿黄铁矿晶体形态和热电性特征对深部含矿性的预测[J].中国地质,40(5):1634-1643.
- 张龙,李胜荣,宋英昕,朱随洲.2020.胶东西北部望儿山金矿床黄铁矿标型特征及找矿意义[J].岩石矿物学杂志,39(2):159-171.
- 张英帅,顾雪祥,章永梅,王佳琳,冯李强,葛战林,何宇.2021.山东蓬莱石家金矿床原生晕地球化学特征及深部找矿预测[J].现代地质,35(1):258-269.